Earth and Planetary Science Letters 394 (2014) 216–228

Contents lists available at ScienceDirect

Earth and Planetary Science Letters

www.elsevier.com/locate/epsl

Strain heating in process zones; implications for metamorphism and partial melting in the lithosphere

Maud H. Devès *, Stephen R. Tait, Geoffrey C.P. King, Raphaël Grandin

Institut de Physique du Globe de Paris, Sorbonne Paris Cité, Univ. Paris Diderot, UMR 7154 CNRS, F-75005 Paris, France

ARTICLE INFO

Article history:
Received 21 November 2013
Received in revised form 27 February 2014
Accepted 2 March 2014
Available online xxxx
Editor: P. Shearer

Keywords:
strain heating
process zone
partial melting
thermo-mechanical model
fault complexities
metamorphism

ABSTRACT

Since the late 1970s, most earth scientists have discounted the plausibility of melting by shear–strain heating because temperature-dependent creep rheology leads to negative feedback and self-regulation. This paper presents a new model of distributed shear-strain heating that can account for the genesis of large volumes of magmas in both the crust and the mantle of the lithosphere. The kinematic (geometry and rates) frustration associated with incompatible fault junctions (e.g. triple-junction) prevents localisation of all strain on the major faults. Instead, deformation distributes off the main faults forming a large process zone that deforms still at high rates under both brittle and ductile conditions. The increased size of the shear-heated region minimises conductive heat loss, compared with that commonly associated with narrow shear zones, thus promoting strong heating and melting under reasonable rheological assumptions. Given the large volume of the heated zone, large volumes of melt can be generated even at small melt fractions.

There are clear examples of volcanism correlated with fault complexities that remain enigmatic and that could be related to that mechanism of "process zone heating". We propose here a simple dislocation model to define the process zones, determine off-fault strain rates and quantify how much plastic work can be dissipated as heat. To provide an example, we examine the case of the junction between the East and North Anatolian shear zones in eastern Turkey. This is chosen because the composition and age of emplacement of the quite extensive volcanics are well known, as are the rates of motion on the associated strike-slip faults. The geometry of the system also allows the dislocation method to be easily adopted. We conclude that melting of the crust and the lithospheric mantle could start only a few Myrs after the onset of deformation. Conservative assumptions for rheological parameters and melting points can explain both the timing and the bimodal nature of the volcanism. Predictions of melt volume are within the rheological uncertainties. While the current paper is focused on strike-slip faults, the approach can be applied to kinematic complexities associated with thrust faults as well, and, maybe more generally, to regions in the lithosphere where oblique boundary conditions force deformation to occur partly in a distributed manner, while still at high rates.

1. The efficiency of strain heating in the lithosphere: a controversy

The spatio-temporal correlation between the emplacement of metamorphic or magmatic bodies and continental deformation suggest an intimate relationship between the thermal and mechanical processes taking place in the lithosphere (e.g. Zhang and Schärer, 1999; Leloup et al., 1999; Jolivet et al., 2003; Rosenberg, 2004; Weinberg et al., 2004; Nabelek and Liu, 2004; Devès, 2010). However, whether lithospheric deformation can of itself produce enough heat to cause high heat flow, high-temperature metamorphism or partial melting in continents is a long-standing debate (e.g. Brune et al., 1969; Yuen et al., 1978; Lachenbruch and Sass, 1980; Ricard et al., 1983; So and Yuen, 2013).

The rate of heat production by dissipation of mechanical work during irreversible deformation (called strain heating) depends on the product of lithospheric strength and strain rate. Whilst enough laboratory data are now available to have a reasonable idea of rock strength, evaluation of the magnitude of strain rate, and of its distribution, is less straightforward. Finite strains within continents do not take place in a homogeneous and steady manner, nor are

* Corresponding author.
E-mail address: deves@ipgp.fr (M.H. Devès).

http://dx.doi.org/10.1016/j.epsl.2014.03.002
0012-821X/

they perfectly concentrated on a finite number of large faults. No model formulation of the relationship between strain and heat has been so far successful in convincingly linking observables of lithospheric deformation with volumes and distributions of magmas produced.

It is common in the literature to distinguish between *frictional heating*, i.e. heat produced during friction on a fault plane in the brittle domain, and *viscous heating*, i.e. heat associated with ductile shearing either on a narrow ductile shear zone or by larger-scale distributed deformation of a viscous lithosphere. Two "end member" approaches have been adopted to model the deformation. One extreme is to assume that the lithosphere can be represented as a viscous fluid subject to the far-field relative plate motion (e.g. England and McKenzie, 1982; Houseman and England, 1986; Kincaid and Silver, 1996). Doing so downplays the heterogeneity of the deformation that is observed at various scales in the field, and notably the occurrence of well-documented tectonic structures, which represent discontinuities in the deformation field that can occur up to the lithospheric scale (e.g. Wittlinger et al., 1998; Armijo et al., 1999; Tapponnier et al., 2001). Another extreme is to assume that continental deformation is characterised by relative motion of a number of rigid blocks along major tectonic boundaries (e.g. Leloup et al., 1999; Rolandone and Jaupart, 2002). In that case, strain heating is focused along well-localised faults or shear zones. In both cases, the strain rate is still fundamentally equal to the velocity applied on the shear zone, or in the far field, divided by the width of the deforming zone. High strain rates are thus predicted for narrow shear zones. For wider zones of deformation, strain rates are lower and predicted heating rates become insignificant (e.g. Kincaid and Silver, 1996; Hartz and Podladchikov, 2008). This has led to the view that narrow shear zones are the most likely places where significant strain heating should occur, and hence where partial melting could take place.

The efficiency of strain heating depends on the competition between the rate of heat production and of weakening of the rocks due to thermal softening. While the exact position of the brittle–ductile transition is quantitatively important, the process is self-limiting overall because the strength of the lithosphere ultimately decreases with increasing temperature. Furthermore, thermal conduction evacuates heat, and is particularly efficient on heat sources like narrow planar shear zones. Models of shear zone heating have incorporated the influence of temperature-dependent thermal diffusivity and heat capacity to increase the efficiency of strain heating by decreasing the ability of the heated lithosphere to conduct heat away; and/or used rheological laws that tend to be less temperature-sensitive, thereby reducing the magnitude of thermal softening (Whittington et al., 2009; Nabelek et al., 2010). However, these advances have not fully closed the gap between model predictions and observations. Models predict relatively moderate temperature increases under geologically reasonable conditions, barely resulting in the generation of very small volumes of magmas (e.g. Leloup et al., 1999). Strain heating is not, therefore, usually considered as a key mechanism in producing the major thermal events that occur coevally with episodes of active deformation.

In this paper, we adopt a new approach by exploring a model in which localised and distributed deformation coexist. We focus on regions where deformation is demonstrably heterogeneous and irreversible while still occurring at high strain rates (Devès et al., 2011). These places are called accommodation zones in structural geology or process zones in material mechanics. In the following we use the term of process zone.

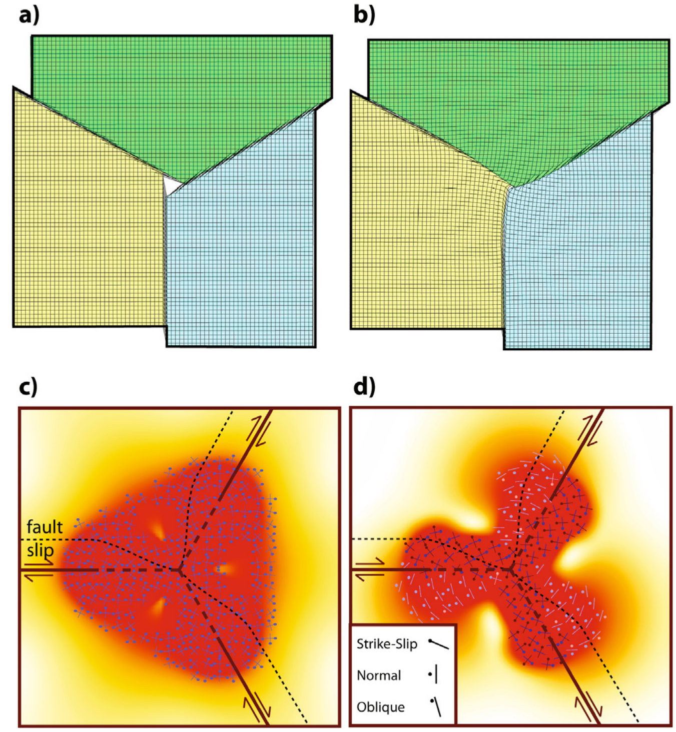

Fig. 1. Process zone of distributed deformation resulting from kinematic incompatibility. The deformation associated with finite motion at a junction between three strike-slip faults can be accommodated in two ways: (a) by opening of a void, or (b) by off-fault deformation when confining pressure prevents large volume changes. Significant shear strains are induced off-faults (reddish colours) (c) under plane strain conditions as (d) under plane stress conditions (for a compressional out of plane principle strain). The short lines shown in (c) and (d) represent the directions of shear predicted within what can be called a process zone. The insert gives the corresponding slip mechanisms. Shear occurs following directions that vary from place to place preventing the development of localised faults or shear zones on long distances. The strain distribution changes between plane strain and plane stress but in both cases, deformation remains distributed with respect to the length-scale of the main faults. The models shown in (c) and (d) have been obtained using a distribution of dislocations in an elastic medium. The figure has been modified from Devès et al. (2011) (see the original paper for more details).

2. A new hypothesis for strain heating

2.1. From kinematic incompatibility to process zones of distributed deformation

Even in the perfectly localised world of plate tectonics, important restrictions on the orientation of plate boundaries or on the relative velocity vectors are imposed by kinematics. Triple junctions are stable only if they allow continuous plate evolution, such as that between three ridges (Fig. 10-3 A, McKenzie and Morgan, 1969). All other possible triple junctions are kinematically unstable and are hence expected to evolve. The question is whether they can always do so whilst respecting their kinematic environment. The Mendocino triple junction for instance has migrated northward in response to the PA-AM-FA plate kinematics, but translation has not accommodated one hundred per cent of the strain. Sliding between the three, allegedly rigid, blocks has been associated with significant distributed deformation (up to about 35%, Field et al., 2013, Table 4). The present paper focuses on that fraction of the strain that cannot be accommodated by translation and localised sliding because of kinematic incompatibility.

An example of an unstable and strongly incompatible triple junction is the point at which three strike-slip faults meet (Fig. 1). The junction cannot evolve stably by translation and localised sliding only. The accumulation of finite motion on the faults requires

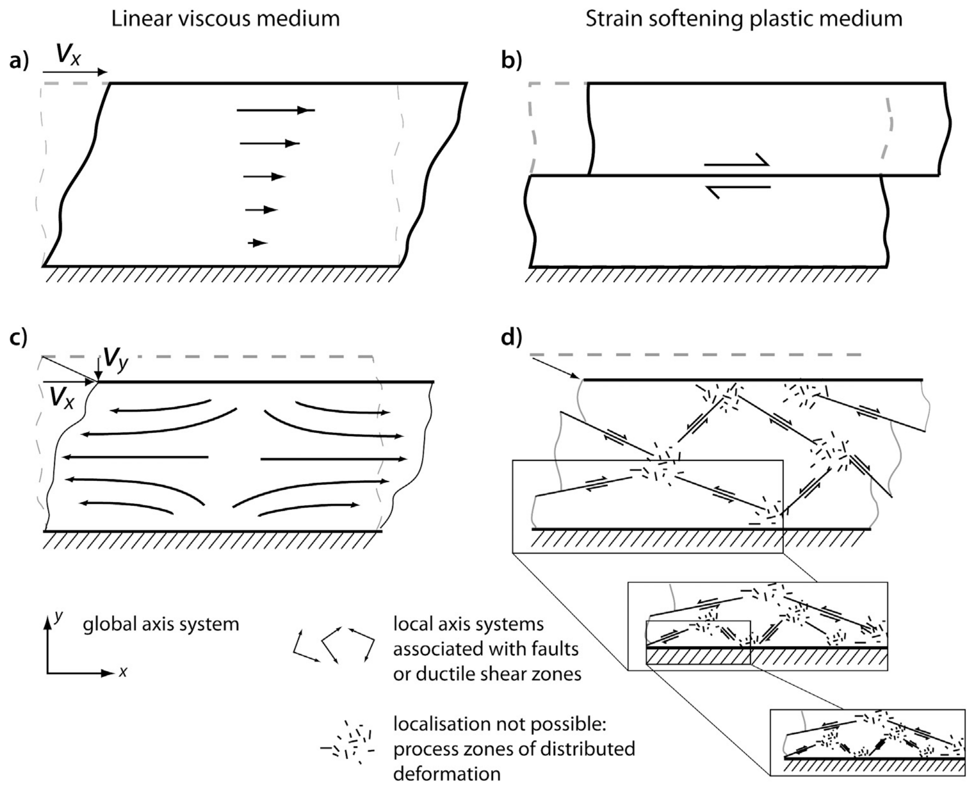

Fig. 2. Kinematic control on the deformation style in strain-softening materials. Schematic view explaining how kinematics can control the co-occurrence of zones of localised and distributed deformation in strain-softening plastic materials. Boundary conditions having a single shear component (a and b) generate a deformation field with a single shear component independent of position (a). In a strain-softening plastic medium like the lithosphere, sliding on a single fault or shear zone can fully release the applied boundary conditions (b), no distributed deformation being required. Most boundary conditions however (c and d) result in more complicated deformation fields whose accommodation requires the creation of faults or shear zones with various orientations. At each scale, the faults apply their own kinematical conditions on the areas they enclose. Process zones of distributed deformation are expected to develop at multiple scales, in fact everywhere the boundary conditions cannot be fully released by sliding on a single localised feature, at all incompatible fault junctions for instance and at ever-smaller scale. The figure has been modified from Devès et al. (2011) (see the original paper for application to the long-term deformation of the Dead Sea region in the Levant).

opening a void at the junction (Fig. 1a). The high confining pressure prevailing in the lithosphere prevents large volume changes, however. Deformation must thus occur off the main faults, in the surrounding blocks, which cannot thus be seen as being rigid (Fig. 1b). The faults correspond to three independent directions of relative sliding. As a result, principal shear directions change from place to place around the junction (Figs. 1c and 1d). This hinders the development of localised features over long distances, or at least on distances of the length-scale of the main faults. Therefore, as finite displacement accrues on the main faults, plastic strain accumulates in a distributed manner in the surrounding medium forming what can be called a process zone.

Oblique boundary conditions in general result in a combination of localised and distributed deformation (Fig. 2). In a linear material subject to simple shear (Fig. 2a), the direction of shear is independent of position. In a strain-softening material, sliding of two rigid blocks on a single localised structure can accommodate the strain (Fig. 2b). The shear zone can acquire substantial displacement without changing geometry, i.e. it is kinematically stable. Such kinematic stability is not possible under oblique boundary conditions resulting in multiple shear zones with different orientations (Fig. 2c). These shear zones in turn impose specific kinematical conditions on the areas they enclose resulting in the development of additional shear zones with different orientations at a smaller scale (Fig. 2d). The same kinematic control applies on the deformation pattern at ever-smaller scales. Deformation of strain-softening materials, such as the lithosphere, is thus controlled by the distant boundary conditions as much as by the local and regional kinematics of faulting, hence process zones are part and parcel of complexly deforming areas.

In the real Earth, oblique kinematics imposed on a plate boundary often lead to the coexistence of (at least) two fault systems, each accommodating one component of the deformation. For instance, the oblique convergence between the Sunda and India plates is accommodated by two nearly parallel fault zones: a subduction megathrust accommodates the trench-normal convergence, while a large strike-slip fault running through the island of Sumatra takes up the trench-parallel component of deformation (e.g. McCaffrey et al., 2000). This extreme example of strain/slip partitioning occurring at lithospheric scale is also visible at the crustal scale. For instance, locations where the direction of a fault strand changes, or where it splits into secondary segments, are often associated with the activation of folds and/or thrusts resulting in a topography (restraining bends) or with pull-apart basins bounded by normal faults (releasing bends) (e.g. Bowman et al., 2003; Cowgill et al., 2004). Although large strike-slip faults, such as those in Anatolia or Tibet, are linear features at a large scale, they invariably host complexities with various degrees of kinematic incompatibility (offsets, bends, intersections with other faults, etc.). These are known to play a key role in nucleating or interrupting earthquake propagation, a behaviour that has been explained by the distributed character of deformation in these areas (King and Nabelek, 1985).

There are many other examples of process zones occurring at various scales and all related to kinematic incompatibility. King and Brewer (1983) explain folding above the Wind River thrust as distributed deformation resulting from kinematic instability induced by the interaction of the thrust termination with the free surface. At a larger-scale, Amelung and King (1997a and 1997b) show that strain in western California is not entirely

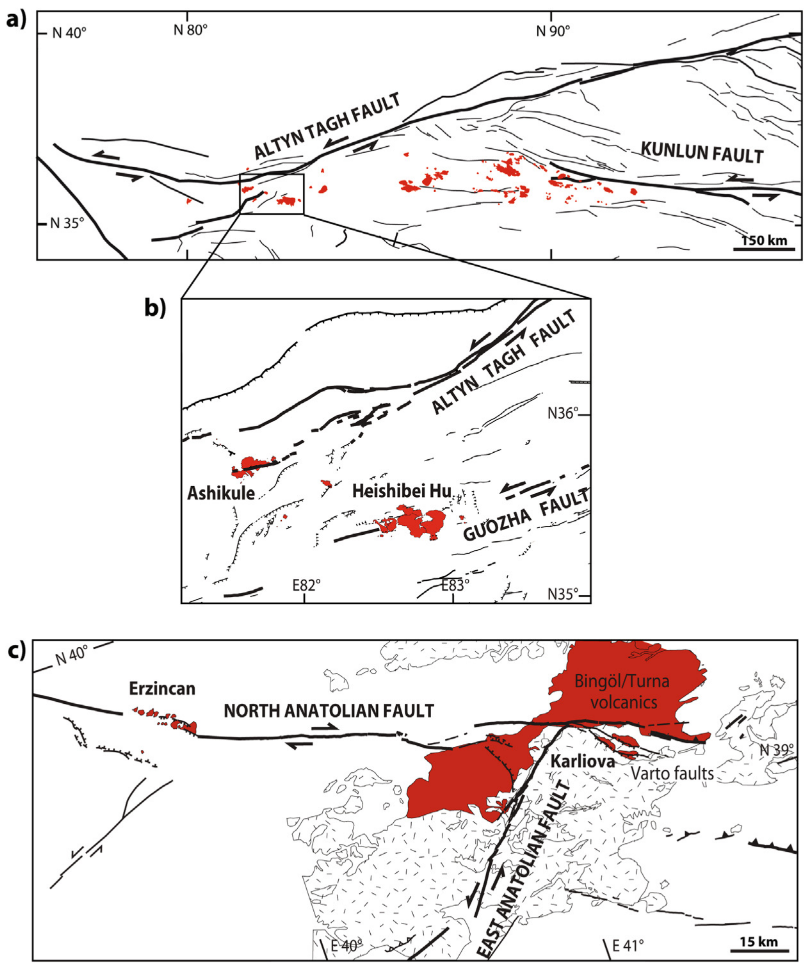

Fig. 3. Patchy volcanism is located in areas of kinematic incompatibilities. In the highly strained collisional areas of Tibet and Anatolia, the volcanism is neither distributed homogeneously nor aligned along the major faults. The lavas are distributed in patches in regions that are subject to kinematical incompatibilities. This figure illustrates this coincidence at various scales. (a) In northern Tibet, a set of volcanic patches occurs at the termination of the Kunlun fault where it interacts with the Altyn Tagh fault system. Other patches occur where the Altyn Tagh fault bends, intersecting another important fault. (b) At smaller scales, the volcanics are again located in zones of kinematic incompatibilities, such as fault bends, offsets and terminations. (c) In eastern Anatolia, there is no volcanism along the straight sections of the North Anatolian and East Anatolian faults. Patches of volcanics occur where the fault system is complicated, at an offset near Erzincan and at the intersection between the two faults near Karliova.

accommodated by localised slip on large well-established faults but also, to a significant extent, by sliding on smaller faults of various orientations, defining a vast process zone of distributed deformation. Devès et al. (2011) show that in the Dead Sea valleys 65% of the strain is localised as slip on the Levant Fault but that kinematic incompatibility forces the remaining 35% to be accommodated in a distributed manner. Experiments of indentation in a plasticine block, that have been used to exemplify the extrusion process due to continental collisions (Peltzer and Tapponnier, 1988), also involve a combination of localised and distributed deformation (discussed in Supplementary Information). The transitory region of complex deformation that precedes propagation of a fault into previously unfractured material has also been called a process zone (Cowie and Scholz, 1992; Armijo et al., 2004, Flerit et al. 2004). Once the fault tip has propagated through a given area, the process zone is expected to become inactive there and to move on with the fault tip. The persistence of process zones through time in given places is more generally determined by the evolution of local and far-field kinematics. As shown by morpho-tectonic studies, some complexities have persisted for several million years while the associated faults have accumulated displacements of tens to hundreds of kilometres (e.g. Karliova junction in Fig. 3, Hubert-Ferrari et al., 2009). In such cases, the process zones are spatially pinned by the larger features of the fault network.

2.2. Spatial and temporal correlation between zones of kinematic incompatibility and patchy volcanism

Fig. 3 shows the distribution of volcanics with respect to major structures of deformation mapped in Northern Tibet and Anatolia. The lavas, although located close to large faults, are not aligned along them. They have been emplaced coevally with active deformation in areas of kinematic incompatibilities (Devès, 2010, Supplementary Information). They preferentially occur in patches at offsets, bends or intersections between several faults or where distinct fault systems interact. This striking spatio-temporal correlation suggests the existence of a physical mechanism relating the occurrence of kinematic incompatibilities with magma generation and transport. Process zones of distributed deformation might well be, as we suggest here, the missing link.

2.3. Can process zones be preferential loci of strain heating?

In the lithosphere, mechanical work can be expended in three main ways: heat generation, creation of new fracture surfaces and, if seismic slip occurs, radiation of elastic waves. Surface energy and seismic energy mainly concern the brittle or semi-brittle portions of the lithosphere and are known to represent only a few percent of the total energy involved in faulting (Scholz, 2002; Chester et al., 2005). Laboratory experiments of shear heating in granites indicate that more than ninety percent of the strain energy is converted into heat (e.g. Lockner and Okubo, 1983). We therefore expect that most of the mechanical work done during irreversible deformation of the lithosphere is converted into heat. In the following, we develop a model to explore the consequences of strain heating in process zones of distributed deformation associated with kinematic incompatibilities.

3. A model for process zone heating

Although a good example to introduce the concept of incompatibility, a junction between three strike-slip faults is an extreme configuration that is not commonly observed in nature, if at all. Intersections between two faults are, on the contrary, very common and are associated with volcanism in numerous cases (Fig. 3). For proof of concept, we therefore take the case of a junction between two vertical strike-slip faults sliding in the opposite direction with uniform slip rates, similar to the geometry of the East and North Anatolian faults (Fig. 3c). There is no problem in principle modelling more complex fault systems provided geometry and rates can be adequately defined (Devès et al., 2011).

3.1. A specific geometry

The use of dislocations embedded in an elastic half-space to represent faults and model the strain associated with motion on them (Okada, 1992) has been extensively and successfully used to calculate surface deformation caused by earthquakes and to compute stress changes associated with a slip event on a given fault system (King and Devès, 2015). This formulation provides a linear approximation to deformation, which is valid as long as the condition of small perturbations is verified (i.e. the magnitude of slip has to be much smaller than the dimension of the fault). As discussed in Section 2, strain localisation cannot occur within process zones on distances that would be comparable to the length-scale of the main faults, precluding large discontinuities in the displacement field at the scale under study. Under such conditions, considering that strain accumulates linearly within a process zone should give good estimates of the mechanical work.

The junction is modelled as two edge dislocations whose contributions are summed. Off-fault strain results directly from the kinematic incompatibility existing between the two faults. The level of incompatibility depends on the junction geometry and kinematics, i.e. on the angles between the faults and on their slip rates. Note that it is equivalent to model the strain using a single edge dislocation whose Burger vector respects kinematic equilibrium with the two other slip vectors. This dislocation represents a missing (or 'phantom') fault, which cannot develop because of the instability of the junction, but whose finite motion would have been able to release the incompatibility (Fig. 4). The strain rate field $\dot{\gamma}$ generated by the intersection of two faults sliding in opposite direction at 2 and 0.9 cm/yr (rates and geometry have been chosen for application in Section 4) is shown in Fig. 4. The strain rate, which is derived from the maximum shear γ, is high close to the fault intersection and decreases with increasing radial distance. Deformation is most intense in two circular lobes joining at the junction.

With each increment of finite motion on the main faults, strain accumulates elastically in the surrounding lithosphere until it reaches a plastic threshold beyond which irreversible deformation commences. We assume that this occurs when the maximum shear strain γ derived from the dislocation model reaches the shear strain obtained at yielding in laboratory experiments γ^{yield}. This plasticity criterion is equivalent to the Tresca criterion. Plasticity occurs by shearing along the plane of maximum shear. Thus,

$$\gamma^{yield} = \frac{\tau}{2G}, \tag{1}$$

where τ is the yield strength (Pa) and G the shear modulus (Pa). The values of the parameters used in the following calculations are reported in Table 1.

At each point where the plasticity criterion has been exceeded, the heat production Q per unit time and volume ($\mathrm{J\,m^{-3}\,s^{-1}}$) is obtained by multiplying the strain rate $\dot{\gamma}$ by the shear strength τ of the lithosphere:

$$Q = \dot{\gamma}.\tau. \tag{2}$$

For a first order estimate, we assume, as many others have (e.g. Leloup et al., 1999; Nabelek et al., 2010), that one hundred per cent of the mechanical work is converted into heat once the plastic threshold has been exceeded.

3.2. Evolution of the rock strength

We adopt the classic approach of strength envelopes developed in the 70s (e.g. Kohlstedt et al., 1995). Laboratory experiments give a measure of the strain rate as a function of applied differential stresses, or vice versa. Extrapolation to the Earth's scale encounters several limitations (Bürgmann and Dresen, 2008) – strain rates in the laboratory are many orders of magnitude larger than those taking place in the lithosphere. Nevertheless it is usually assumed that the laws derived from laboratory experiments are a good representation of the strain–stress behaviour that a medium of similar composition would have under other loading conditions. The shear strength τ at a given depth is thus the smallest between the brittle strength τ_f and the ductile strength τ_d predicted by experimentally determined constitutive laws.

The stress required to fracture an intact rock is substantially higher than that required to initiate sliding on pre-existing faults (e.g. Paterson and Wong, 2005). Given the ubiquity of localisation in strain-softening materials and bearing in mind that distributed deformation within process zones can occur by sliding on multi-scale faults, it seems reasonable to consider the frictional strength as a minimum estimate to the brittle strength. Byerlee's law (1978) relates the frictional strength to the normal stress σ_n (in MPa) as follows:

$$\tau_f = 0.85\sigma_n, \tag{3}$$

at confining pressure under 200 MPa,

$$\tau_f = 0.6\sigma_n + 50, \tag{4}$$

at higher confining pressure.

The effective normal stress σ_n is taken equal to the lithostatic pressure $P = \rho g z$ assuming no effect from pore fluid pressure. ρ is the density, g the acceleration of gravity and z the depth.

Once ductile deformation begins, it is often considered that dislocation creep processes control macroscopic lithosphere behaviour (Ashby and Verrall, 1978; Bürgmann and Dresen, 2008). The corresponding constitutive laws can be expressed in the following form:

$$\Delta\sigma = A^{-\frac{1}{n}}.\exp\left(\frac{E+PV}{nRT}\right).\dot{\gamma}^{\frac{1}{n}}, \tag{5}$$

where A is a pre-exponential constant ($\mathrm{Pa^{-n}\,s^{-1}}$), E the activation energy ($\mathrm{J\,mol^{-1}}$), R the universal gas constant (8.32 $\mathrm{J\,mol^{-1}\,K^{-1}}$), V the activation volume ($\mathrm{m^3}$), P the pressure (Pa), T the absolute temperature (K) and n is an integer accounting for the nonlinearity of the response of the strength and $\dot{\gamma}$ the strain rate. The shear strength τ_d is obtained by dividing the differential stresses $\Delta\sigma$ by 2. Bürgmann and Dresen (2008) and Karato (2008) provide a compilation of power flow laws obtained for synthetic mineral aggregates or natural rock samples under various fluid environments. The strain rate used to calculate the ductile strength is derived from the dislocation model. In this example where the faults

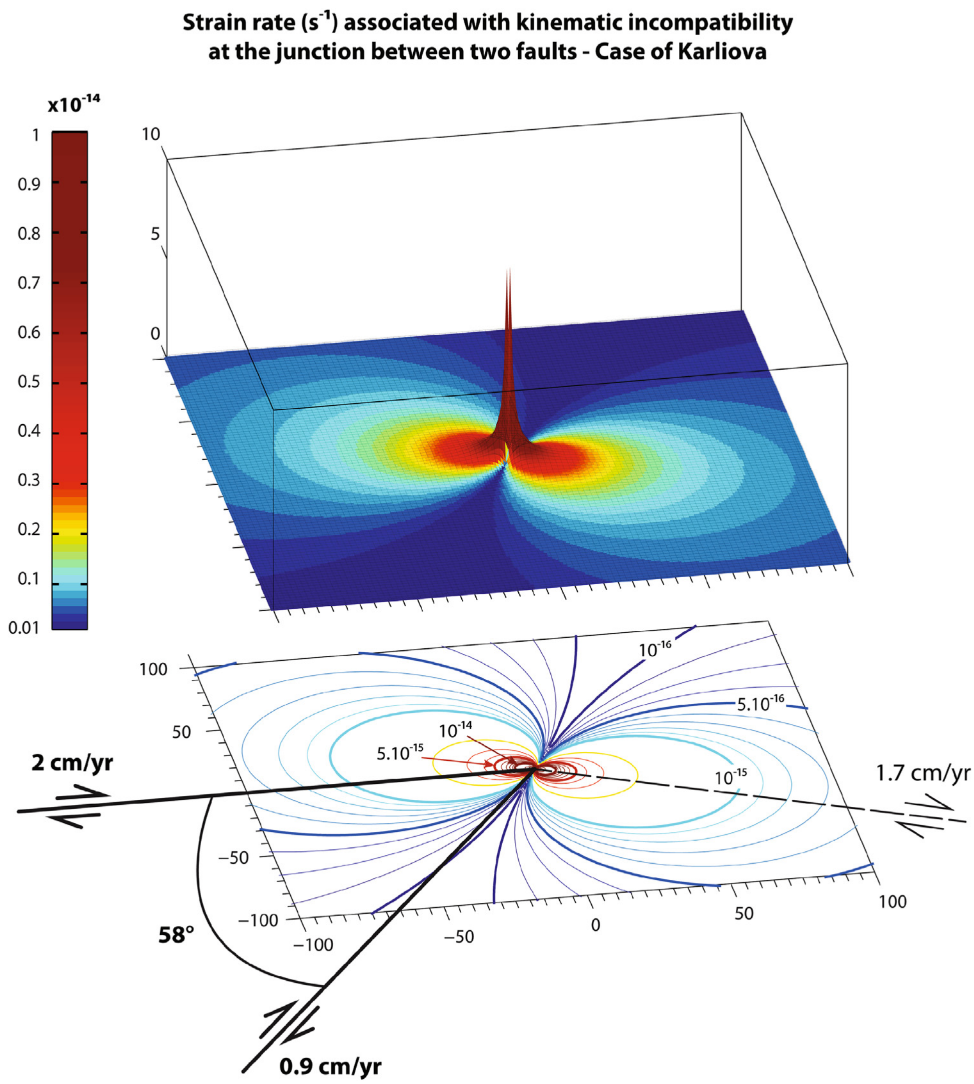

Fig. 4. Strain rate model at a strike-slip/strike-slip junction. Strain rate field associated with the tip of a vertical strike-slip fault sliding at 1.7 cm yr^{-1}. It is equivalent to that modelled for Karliova junction (Section 4) where the right-lateral NAF, sliding at 2 cm yr^{-1}, intersects with the left-lateral EAF, sliding at 0.9 mm yr^{-1}, at an angle of 58°. The strain rate is derived from the second invariant of shear. Under plane strain conditions, the latter corresponds to the component of maximum shear that can be calculated in each point of the horizontal plane (King and Devès, 2015). Poisson's ratio is 0.4. Note that dividing Poisson's ratio by 2 would decrease the amplitude of the maximum shear strain by only 25% whereas multiplying the displacement applied on the fault by 2 would double it. The sensitivity of the strain rate to changes in Poisson's ratio hence remains small. We use the standard value of 0.4 in the calculations of Section 4.

Table 1
Model parameters.

Parameters	Symbol	Value	Units
Poisson coefficient	ν	0.4	
Standard gravity	g	9.81	$m^2\,s^{-1}$
Depth of the Moho	M_z	40	km
Depth of the lithosphere–asthenosphere boundary (LAB)	L_z	130	km
Specific heat capacity	C_p	1000	$J\,kg^{-1}\,K^{-1}$
Surface temperature	T_0	20	°C
Heat flow at the LAB	Q_b	20	$mW\,m^{-2}$
Crust			
Density	ρ_c	2800	$kg\,m^{-3}$
Shear modulus	G_c	3×10^{10}	Pa
Thickness of the enriched upper crust	h	10	km
Radioactive heat production in the upper crust (h)	A_{uc}	3.27	$\mu W\,m^{-3}$
Radioactive heat production in the lower crust (h)	A_{lc}	0.35	$\mu W\,m^{-3}$
Conductivity	k_c	2.5	$W\,m^{-1}\,K^{-1}$
Mantle			
Density	ρ_m	3300	$kg\,m^{-3}$
Shear modulus	G_m	6×10^{10}	Pa
Radioactive heat production	A_{mantle}	0.02	$\mu W\,m^{-3}$
Conductivity	k_m	3	$W\,m^{-1}\,K^{-1}$

are vertical and the deformation considered to be plane strain, the maximum shear strain is equal to the second invariant of the strain tensor. Strain rate varies spatially but, at each point, does not vary with time. On the contrary, the ductile shear strength, and thus the strength profile, evolves during iterations as temperature increases.

3.3. Solving the heat flow equation

We now solve the heat flow equation to assess the temperature field associated with process zone heating. For simplicity, we discuss the problem within the geometrical framework described above, but the fundamental arguments can be generalised. Although there are configurations under which advection could play a role, one can consider that highly incompatible junctions are associated with highly non-collinear shear directions preventing efficient displacement of material away from the heating zone. The influence of heat advection is hence neglected at this stage. The equation of heat balance can thus be written:

$$\rho.C_p.\frac{\partial T}{\partial t} = k.\nabla^2 T + Q + Q_r, \tag{6}$$

where ρ is the rock density ($\mathrm{kg\,m^{-3}}$), C_p the specific heat capacity ($\mathrm{J\,kg^{-1}\,K^{-1}}$), T is the temperature in degrees Kelvin (K), t is the time (s), k is the conductivity ($\mathrm{W\,m^{-1}\,K^{-1}}$), Q the heat generation per unit time and unit volume ($\mathrm{J\,m^{-3}\,s^{-1}}$) due to strain heating within the process zone and Q_r the radiogenic heat generation ($\mathrm{J\,m^{-3}\,s^{-1}}$). Radiogenic heating occurs at much slower rates and, although it enters the calculations shown here, its influence is not discussed.

Here we derive a dimensionless form of Eq. (6) to estimate the balance between the rate of heat production by strain heating and the rate of the heat lost by diffusion. Dividing the characteristic size of the process zone by the velocity of the faults gives a natural time scale to the problem. It is not straightforward however to estimate that characteristic size. Contrary to what has been assumed in classical models of shear heating on shear zones, the heat source is no longer a plane. The plastic process zone (as defined by Eq. (1)) grows in proportion to the rate at which the main faults slide. However, the impact of process zone heating on the thermal equilibrium of the lithosphere depends less on the total extent of the plastic zone than on the size and shape of the sub-zone within which significant heat is produced. In our example, the strain rate field does not vary with depth (Fig. 4). The contours, which define two circles joining at the point of the dislocations, therefore extend as cylinders in the z-direction. But the strength varies with depth and time, *via* its dependency on temperature. The deformed process zone therefore acts as a volumetric heat source, whose vertical extent and power evolve with time.

For an approximately cylindrical source, it is reasonable to consider the radial and vertical directions for evaluating the importance of thermal diffusion. Two characteristic length scales are hence introduced: a horizontal scale, L_p, and a vertical scale, D. The details of the heat production in the immediate vicinity of the dislocations are not of primary importance – diffusion will smooth out the steepest gradients of the heated zone. For the purpose of scaling, we therefore take L_p to be the distance from the junction to the farthest point at which a chosen strain rate is attained (Fig. 4). This has the advantage of being constant for a given calculation. Because we will ultimately be interested in whether rocks can be raised to their solidus, we scale temperature with the difference between the solidus temperature (T_{sol}) and an initial reference temperature (T_0). To derive a dimensionless equation, we use the following scales:

$$r = r'.L_p, \tag{7}$$

$$z = z'.D, \tag{8}$$

$$t = t'.\frac{L_p}{V}, \tag{9}$$

$$T = T'.(T_{sol} - T_0). \tag{10}$$

The dimensionless form of Eq. (6) is thus:

$$\frac{\partial T'}{\partial t'} = L'.\left[\frac{1}{r'}.\frac{\partial}{\partial r'}\left(r'.\frac{\partial T'}{\partial r'}\right) + R'^2.\frac{\partial^2 T'}{\partial z'^2}\right] + Q'. \tag{11}$$

Three dimensionless numbers have appeared:

$$L' = \frac{\kappa}{L_p.V}, \tag{12}$$

$$R' = \frac{L_p}{D}, \tag{13}$$

$$Q' = \frac{L_p}{\rho C_p V (T_{sol} - T_0)} Q, \tag{14}$$

where Q' measures the rate of strain heating relative to the thermal inertia of the medium. L' (which weights the diffusive term) has the form of the inverse thermal Peclet Number encountered in fluid mechanics. It is not here the comparison of the rates of advection and diffusion of heat but the ratio of the time scale of strain heating (L_p/V) versus the horizontal diffusive time scale (L_p^2/κ). If L' is small with respect to 1, horizontal diffusion cannot balance the heat production term and temperature must increase. For a fault sliding at $V = 1\ \mathrm{cm\,yr^{-1}}$, and with $\kappa = k/\rho C_p = 9 \times 10^{-7}\ \mathrm{m^2\,s^{-1}}$, the characteristic size of the process zone must be larger than 3 km for L' to be smaller than 1. Significant tectonic deformation generally occurs for strain rates larger than $10^{-15}\ \mathrm{s^{-1}}$ (average plate motion). It is hence likely that, despite the theoretically unlimited growth of the plastic process zone, the portion of the process zone that is significantly deformed, and heated, is that deforming at strain rates larger than $10^{-15}\ \mathrm{s^{-1}}$. Considering the $10^{-15}\ \mathrm{s^{-1}}$ contours shown in Fig. 4, L_p is more typically of the order of several tens of km. We can therefore conclude that thermal diffusion should smear out steep horizontal gradients within the process zone but be relatively ineffective in removing heat from the process zone associated with major faults sliding at rates of the order of a $\mathrm{cm\,yr^{-1}}$.

R' quantifies the influence of the aspect ratio of the heated zone on the efficacy of the heat loss by diffusion in the vertical direction with respect to that occurring in the horizontal plane. Horizontal diffusion is weighted by L', which is small at all times, whereas the vertical diffusion term is multiplied by $L' \times R'^2$. The initial steady geotherm already incorporates a vertical gradient, to which strain heating adds a perturbation. Because the source is originally smaller in the horizontal direction than in the vertical, horizontal diffusion should initially have a larger influence than vertical diffusion on the evolution of the temperature perturbation. However, because ductile strength depends on temperature, heat production varies with depth and time. D is the characteristic scale of vertical temperature gradients. If it is taken to represent the depth of the brittle–ductile transition, where the heat production will be maximum at all stages, it is expected to decrease as thermal softening proceeds. R' hence increases with time and might become large enough to outweigh the low value of L'. Therefore, although horizontal thermal diffusion appears to be of greater importance than vertical diffusion at early stages of the heating process, one can expect the latter to take over with time. Horizontal diffusion is therefore neglected in our calculations, but not vertical diffusion. The following results validate this approach.

4. Application to Karliova junction

The junction between the North Anatolian fault and the East Anatolian fault provides a good example of a kinematically incompatible junction that is associated with volcanism (Fig. 3).

Table 2
Power flow laws parameters used to calculate the ductile strength.

	A ($Pa^{-n}\ s^{-1}$)	n	E ($kJ\ mol^{-1}$)	V ($m^3\ mol^{-1}$)
Crust				
Anorthite dry (Rybacki et al., 2006)	5.01×10^{-6}	3	641	2.4×10^{-5}
Cpx dry (Bystricki and Mackwell, 2001)	3.98×10^{-19}	4.7	760	-
Quartzite dry (Ranalli and Murphy, 1987)	2.5×10^{-20}	2.4	156	–
Albite dry (Ranalli and Murphy, 1987)	1.03×10^{-29}	3.9	234	–
Mantle				
Olivine dry (Karato and Wu, 1993)	6.03×10^{-23}	3.5	540	2×10^{-5}
Olivine dry (Korenaga and Karato, 2008)	2.81×10^{-24}	4.94	610	1.3×10^{-5}

Hubert-Ferrari et al. (2009) distinguish between two periods of volcanism: a 7 to 4 Ma stage, characterised by a bimodal distribution of mafic and acid products, dominated by mafic lavas, and a more recent stage corresponding to the construction of the Bingöl/Turna volcano (∼3 Myrs ago) and to the emplacement of small volcanic domes around Varto (∼3 to 0.5 Myrs ago), all characterised by intermediate lavas. The first stage of volcanism, although undoubtedly associated with significant deformation rates due to the collision between the Arabian and Eurasian plates, may have preceded the establishment of clear through-going faults in the region. The second stage was coeval with faulting on the North and East Anatolian faults. The volcanism covers a zone of complicated deformation comprising fault branching, horsetail and reverse faulting; all features that are typical of a damage pattern occurring at the tip of strike-slip faults and reveal the occurrence of distributed strain in the region (Hubert-Ferrari et al., 2009).

The volume of the Bingöl/Turna volcano is about 800 km^3 (maximum estimate from the topographic profile drawn by Hubert-Ferrari et al., 2009 and a georeferenced map of the surface covered by the volcanics). Petrological and geochemical data, together with the presence of basaltic enclaves in Varto domes (Buket and Temel, 1998), suggest mixing of crustal and lithospheric mantle derived magmas (compilation in Devès, 2010). The silicic lavas of Bingöl/Turna and Varto are depleted in incompatible trace elements compared with the mafic ones, which precludes a fractional crystallisation relationship of the two lava suites (Pearce et al., 1990; Buket and Temel, 1998).

4.1. Modelling

We model the North and East Anatolian faults as two straight, vertical dislocation planes running through all the lithosphere. Accordingly to offset morphology, geodetic data and regional kinematic models, we set their average slip rates at, respectively, 20 and 9 $mm\ yr^{-1}$ (McClusky et al. 2000 and 2003, Reilinger et al., 2006; Hubert-Ferrari et al., 2002, 2009). The angle of intersection between the two faults is 58°. Kinematic incompatibility at the junction may have been partly released by localised sliding on the strike-slip and normal structures of the Varto fault system, which run in continuation of the NAF, and by more or less well-localised deformation on the fold-and-thrust system of Mus (Supplementary Information). There is no evidence however that these structures were active before the eruption of the voluminous Bingöl/Turna volcanics. It seems therefore reasonable to neglect them while modelling strain heating. Their contribution to the regional deformation is poorly constrained but should anyway remain small compared to the contribution of the large North and East Anatolian faults (Hubert-Ferrari et al., 2002).

There are few constraints on the thermal structure of the Anatolian lithosphere. Surface heat flow values are often very high (Ilkiçsik, 1995) because of transient perturbations due to active tectonics and magmatism. Although the geotherm is known to vary with the regional geology, it is reasonable to adopt an average approach when looking at the lithospheric scale (Jaupart and Mareschal, 2007). The initial geotherm is thus calculated by integrating the heat equation considering that the crust is made of an enriched upper crust extending over 10 km and extends down to the depth of 40 km where seismic studies locate the Moho (Zor et al., 2003; Angus et al., 2006). We use average estimates for the radiogenic heat production in the lower crust and the mantle (Table 1). We fix the heat flux at the bottom of the lithosphere rather than the temperature – i.e. the lithosphere–asthenosphere boundary is modelled as a diffuse rather than a sharp thermal boundary. We assume that the conductivities in the crust and the mantle do not vary with temperature during the heating process, which leads to slight underestimates of the temperature. These assumptions do not affect however the validity of our conclusions.

4.2. Results

The process zone deforms at rates comprised between 10^{-16} and more than $10^{-14}\ s^{-1}$ (Fig. 4). Calculations have been undertaken considering a variety of power flow laws for the ductile strength. In the continental context under study, partial melting is likely to occur in the absence of an excess of fluids. We hence settle for showing the results obtained for dry rheologies (Table 2). For illustration, we show the results corresponding to extreme rheologies in the mantle (the olivine1 law, from Karato and Wu, 1993, proves to be one of the hardest over time, the olivine2 law, from Korenaga and Karato, 2008, is one of the softest). We consider a variety of laws in the crust in order to account reasonably for the expected geological heterogeneity. Clinopyroxenite (Cpx) and quartzite laws correspond to extreme cases (Cpx is very hard, Quartzite is very soft). Anorthite and albite are intermediate cases (anorthite being the strongest of the two). The temperature profiles are compared with those of muscovite, biotite and amphibole break-down, corresponding to dehydration melting in the crust, and with those of peridotites containing trace amounts of water trapped in 'anhydrous' minerals, corresponding to dehydration melting in the mantle.

Fig. 5 shows the evolution of temperature and strength with depth and time for distinct strain rate values for a given strength profile (anorthite in the crust and olivine1 in the mantle). Higher strain rates are associated with larger temperature rise (Fig. 5a). Higher rate of heat generation however lead to a faster decrease in heating efficiency due to thermal softening (Fig. 5b). The competition between heating and thermal softening controls the occurrence of partial melting. As temperature increases, the depth of the brittle–ductile transition decreases, changing the shape of the heated zone over time (Fig. 5b). Fig. 6 shows the temperature and strength profiles obtained after 5 Ma of process zone heating for different rheological profiles. Comparison of the results obtained for two olivine creep laws in the mantle (green and magenta curves), *a priori* obtained under similar experimental conditions, show that the rheological uncertainties are large. These uncertainties affect all models of strain heating however

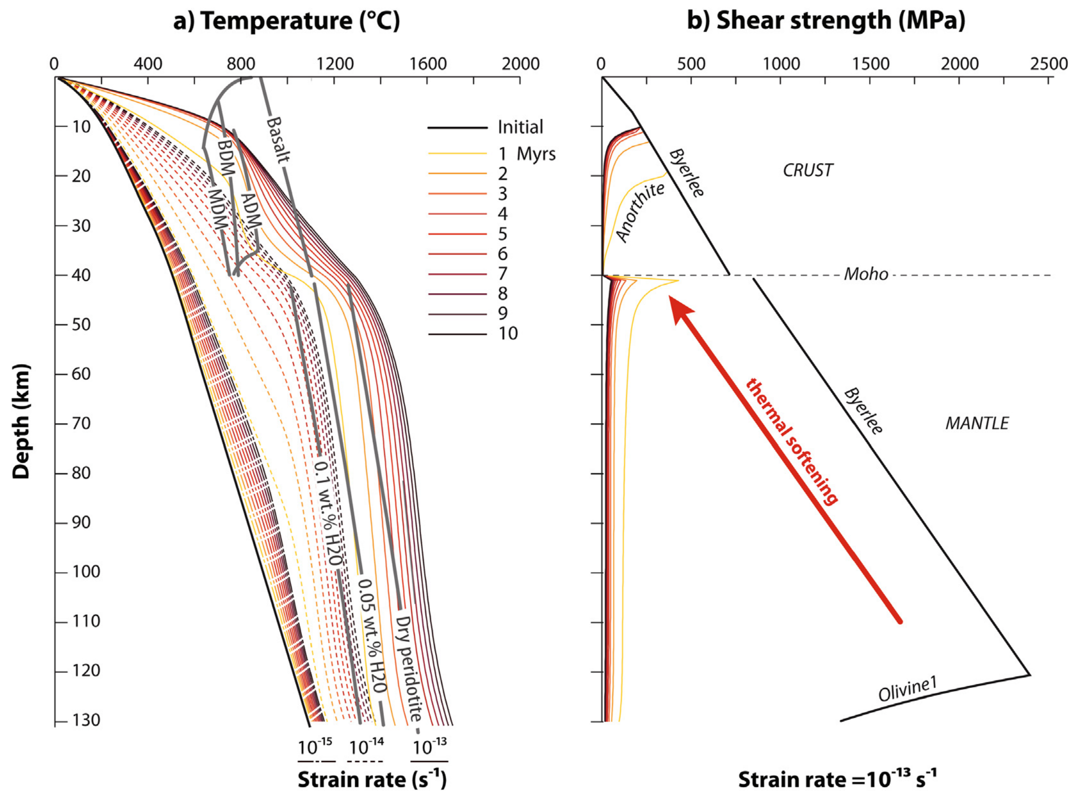

Fig. 5. Temperature and strength profiles for strain heating at various rates, with vertical diffusion. (a) Temperature profile versus depth, time and strain rate. The initial geotherm is the solid black line. Temperature profiles are drawn for 3 distinct strain rate values: 10^{-15} (hatched lines), 10^{-14} (dotted lines), and 10^{-13} s^{-1} (plain lines). The line colour evolves from yellow to brown with time. Melting starts when temperatures reach the solidi that are represented by the thick grey curves. In the crust, melting takes place by breakdown of hydrous minerals such as muscovite, biotite (MDM and BDM, Thompson and Connolly, 1995) and amphibole (ADM, Lopez and Castro, 2001). The dry basalt solidus is also shown for illustration. Melting curves of a dry peridotite or a peridotite that contains 0.05 and 0.1 wt% of water are shown in the mantle (Katz et al., 2003). Assuming a partition coefficient of 0.01 between the rock and the melt, the resulting melt would contain 5 to 10 wt% of water at the onset of melting, an amount that would rapidly decrease with increasing melt fractions. (b) Strength profile versus depth and time for a strain rate of 10^{-13} s^{-1}. As in (a), the line colour evolves from yellow to brown with time. The strength is derived from Byerlee's law in the brittle domains of the lithosphere and from dislocation creep laws of dry anorthite (Rybacki et al., 2006) and dry olivine (Karato and Wu, 1993) in the ductile domains of, respectively, the crust and the mantle. Ductile deformation becomes easier and easier as the temperature increases and takes over from brittle deformation at ever shallower depths. (For interpretation of the references to colour in this figure legend, the reader is referred to the web version of this article.)

and are not specific to our model. Overall, one can conclude that strain heating is more efficient in the crust if the rheology of the ductile layers is dominated by, in order of efficiency, clinopyroxenite, anorthite, albite and quartzite. The quartzite/olivine1 profile (yellow curve) illustrates well that the heat generated in a strong upper mantle can diffuse upward and heat a weaker, but potentially more fertile, lower crust. This assumption is made by Leloup et al. (1999) to account for melting on narrow shear zones. We will see however that it is not necessary to explain significant melting in our case. It is important to outline however that the mineral assemblages generating the most heat (i.e. with a rheology less sensitive to thermal softening) are not necessarily the ones that are expected to melt first. The lithosphere is highly heterogeneous and rheological strong rocks are likely to co-exist with rocks containing mineral assemblages whose break-down can lead to melt at a lower temperature than their own melting temperature. For strain rates on the order of or higher than 10^{-14} s^{-1}, Figs. 5 and 6 show that melting temperatures can be reached within few Myrs in both the crust and the mantle.

In the horizontal plane, the heated zone expands quickly with time and is always larger than the surface through which heat could be diffused away (Fig. 7). The regions where the melting temperature has been exceeded are contoured in blue (for the rheologies and melting curves as specified). The brown circles show that the effect of horizontal diffusion can be neglected at this stage of proof of concept. It would smooth out the temperature maps where the gradients are sharpest but would not modify the results at first order.

Fig. 8 shows the temporal evolution of the volume of crustal and mantle rocks whose temperature exceeds their melting point, under various assumptions. These volumes are not directly representative of the volumes of magmas that can be erupted. Only a fraction is expected to melt depending on the amplitude of the temperature increase above the melting curves, on the composition of the rock, on its fertility and on the fluid regime. Some of the melting products may also be left behind during extraction and transport toward the surface. Considering melt fractions comprised between 50 and 10%, a volume of 1600 to 8000 km^3 must be brought at the point of melting to produce a volume of magma of 800 km^3 – our estimated upper bound for Bingöl/Turna volcanism. The model predicts that this can be achieved by melting of the mantle for a peridotite containing 0.2 wt% H_2O in less than 1 to 2 Myrs, for a peridotite containing 0.1 wt% H_2O in less than 4 to 8 Myrs, for peridotite with a smaller water content in more than 10 Myrs. It can also be achieved by melting of the crust, for anorthite and muscovite break-down or cpx and biotite break-down in less than 6 to 10 Myrs, for anorthite and biotite break-down in less than 8 to 10 Myrs. It would take more time considering quartzite or albite rheologies with the muscovite break-down curve.

The lavas testify to mixing between crustal and mantle magmas. Independent but coeval melting of pertinent volumes of the crust and the mantle are achieved within 4 to 7 Myrs considering biotite break-down and a 0.1 wt% H_2O peridotite. It occurs within

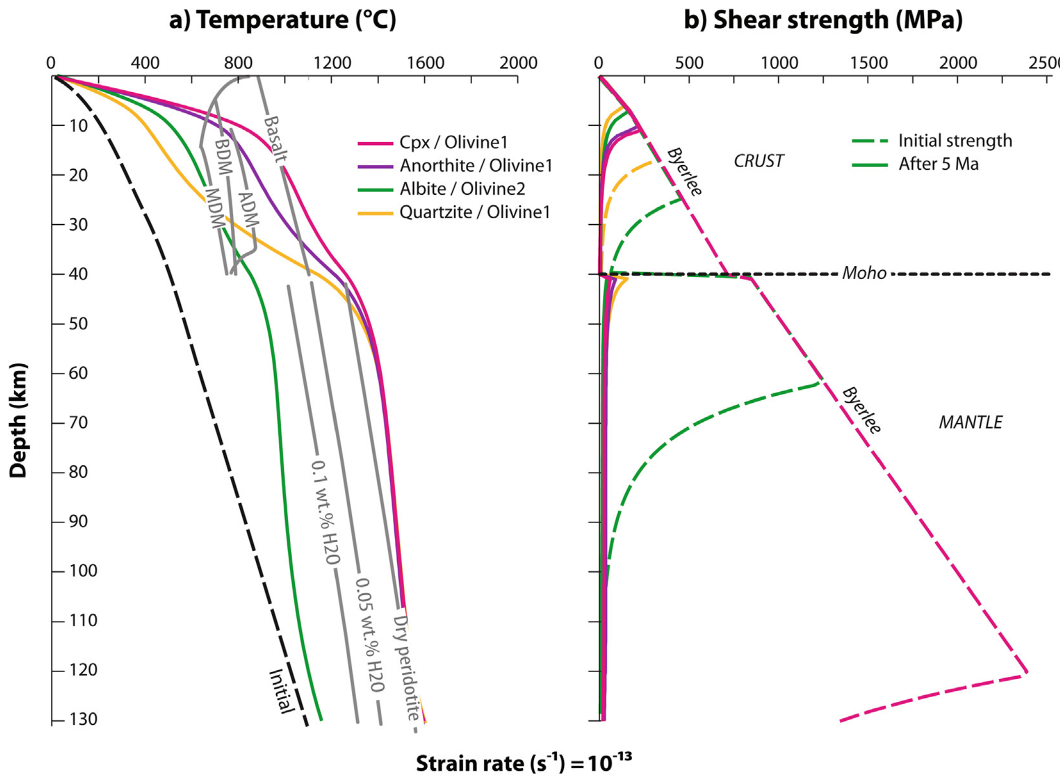

Fig. 6. Temperature and strength profiles after 5 Myrs of process zone heating at a strain rate of 10^{-13} s^{-1} for various rheologies (Table 2). The dotted lines correspond to the initial state. The grey lines correspond to the same melting curves as in Fig. 5. Comparison between two olivine laws illustrates well the rheological uncertainties associated with all models of strain heating. According to Korenaga and Karato, 2008, activation energy and stress exponent are the only parameters of the dislocation creep laws that can be assessed with accuracy from experiments. The dependence of power flow laws on water content is particularly poorly resolved, because of technical difficulties in assessing the true water content in experiments. Even less well resolved is the influence of pressure. The parameter *A* is ill defined: as calculated, it can vary by several orders of magnitude for a small change in activation energy (Stocker and Ashby, 1973).

3 to 6 Myrs for muscovite break-down. It occurs within 1 to 2 Myrs for a 0.2 wt% H_2O peridotite. The model can therefore account for the bimodality of the lavas within the rheological uncertainties.

Bingöl/Turna volcanism is 3 Myrs old. This requires, in the best case, that the North and East Anatolian faults were established in the area 4 to 5 Myrs ago. Although the faults have been active in the last 3 Myrs (they have demonstrably offset the volcanic cover since then), there is no clear evidence for when faulting was initiated. It has been proposed that the development of the current North and East Anatolian Faults could have occurred co-evally with a large scale tectonic rearrangement 5 ± 2 Myrs ago (e.g. Armijo et al., 1999; Hubert-Ferrari et al., 2009). The model predictions fit well within the scenario of a two-stage deformation process. The older phase of volcanism dated between 7 and 4 Myrs may well correspond to the former phase of deformation, although that is difficult to test quantitatively. There is evidence that structures become established first in the mantle lithosphere and later propagated into the crust, which could provide an explanation for the earlier and more mafic character of that volcanism (e.g. Hubert-Ferrari et al., 2003).

Given the uncertainties in the rheology, which affect all models of strain heating, it is difficult to discuss timing, melt fractions and volumes in more detail. We can however compare our model with previous ones. Shear heating on a planar fault/shear zone sliding at 4 $cm\,yr^{-1}$ (double than our case) is expected to lead to partial melting of the lower crust only (Leloup et al., 1999, by melting of the fertile lower crust due to heat diffused from a strong hot upper mantle). The muscovite break-down curve is exceeded over at best 5 km. Considering a 1 km-wide and 100 km-long shear zone, this means that only 500 km^3 of crust can exceed its melting point (1000 km^3 for a 1 000 km-long segment). Such volumes, calculated at steady-state, are at least an order of magnitude lower than the volumes obtained with process zone heating in a much shorter time-lag. Models of strain heating along linear structures moreover do not explain the patchy distribution of volcanism at fault complexities.

5. Discussion

The usual objection to strain heating playing a major role on lithosphere thermo-mechanics is that it is, by essence, limited by thermal softening in narrow shear zones, whose geometry allow effective conductive cooling. In process zones however, heat is produced over large volumes. This implies that the heat loss by conduction is negligible when faults slide at rates of a few $cm\,yr^{-1}$. Our simulations demonstrate that temperature increases rapidly leading, under certain conditions, to partial melting of the crust and the mantle of the lithosphere only a few Myrs after the onset of deformation. The large volume of the process zones also ensures that large volumes of magmas can be generated even at small melt fractions. There are large rheological uncertainties but those are the same for all models of strain heating. Process zone heating is more efficient than shear heating on faults or shear zones and is liable to produce significant volumes of magmas much more rapidly.

Large volumes of magmas can only be produced if the kinematic complexity is maintained for sufficient time, which appears to be the case at Karliova. Although it is clear that magmas can be produced on time scales short with respect to the evolution of the large-scale and local kinematics, there are places where the evolution of the kinematics of the system is expected to affect the timing of the heating process, the composition and the volumes of magmas.

We have assumed that localisation does not occur within the process zone, or at least not on length-scales that are significant

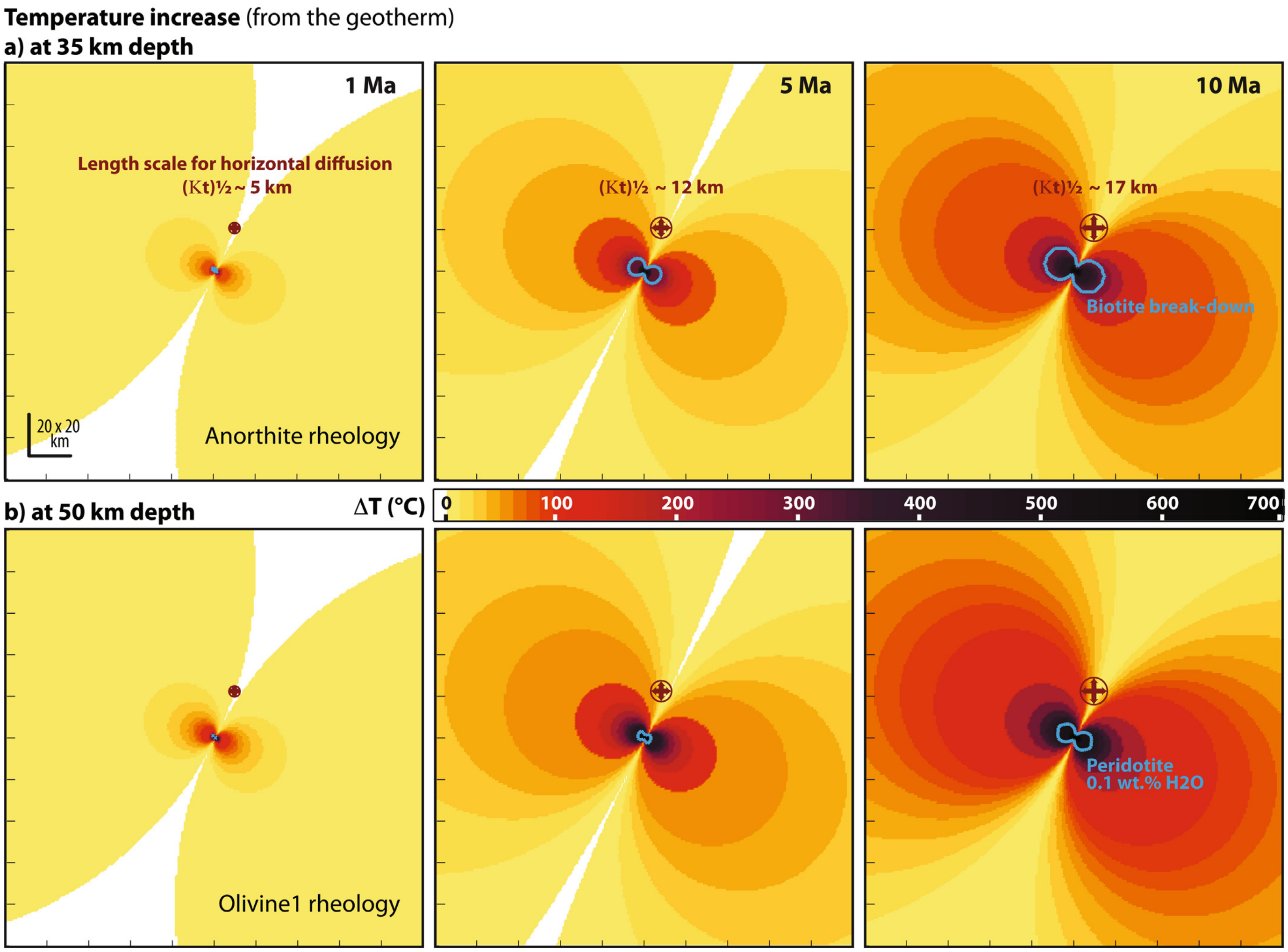

Fig. 7. Maps of temperature increases obtained after 1, 5 and 10 Myrs of process zone heating at 35 and 50 km depths, respectively in the lower crust and the upper mantle. The blue contours show the areas where the temperature of melting are exceeded; for biotite dehydration melting in the crust and melting of a peridotite containing 0.1 wt% of water. (For interpretation of the references to colour in this figure legend, the reader is referred to the web version of this article.)

with respect to the length-scale of the main faults. This might not be completely true. Taking localisation into account is however computationally challenging and some degree of localisation should not significantly affect the heat budget estimated here.

Horizontal diffusion should be added in a future model. As shown however, it should not affect much estimates made for major faults. It will moreover tend to counteract thermal softening by delaying attainment of the brittle–ductile transition in the hottest part of the process zone, while remaining ineffective at cooling the whole zone.

The success of our calculation regarding Karliova volcanism suggests that process zone heating associated with highly incompatible complexities (such as fault terminations, significant offsets, high angle intersections) on faults sliding at rates of $\mathrm{cm\,yr^{-1}}$ could be a quite general process to generate substantial volumes of magmas. The extent of the process zones, the duration after which melting can start and the volumes of the zones that are melting would vary with the level of incompatibility of the complexities and with the rheology and the melting curves that are considered.

Part of the rationale for choosing Karliova junction in this illustrative calculation is that there is no obvious mechanism for partial melting associated with strike-slip faults (apart from strain heating). Volcanism at places such as Karliova, in fact volcanism occurring in collision zones more generally, has defied satisfactory explanation. The isotopic signature of the lavas suggests melting of the crust and the mantle of the lithosphere, with no clear contribution of the convecting asthenosphere (e.g. Pearce et al., 1990 for Anatolia, Turner et al., 1996 and Miller et al., 1999 for Tibet). Previous models of delamination (e.g. Morency and Doin, 2004), of convective removal of the lower lithosphere (e.g. Conrad, 2000), of slab break-off (e.g. Van Hunen and Allen, 2011), cannot account for this geochemical signature, nor they can explain the coeval migration of volcanism with deformation at different stages of the collision (Devès, 2010). Process zone heating can explain the genesis of large amount of mantle melts in the lithosphere, without having to invoke heat or melt contributions from the asthenosphere. The combination of crustal melting, differentiation of mafic end-members and mixing of crustal- and mantle-derived melts can result in a wide range of magma compositions. Silicic and intermediate lavas could be more abundant than mafic lavas under some circumstances, a puzzling feature observed in collisional context (Devès, 2010). Modelling how kinematical boundary conditions can drive distributed shear heating at continental scale is beyond the scope of the present paper. Some boundary conditions may play, however, a similar role to fault complexities in forcing the deformation to occur in a distributed manner while still at high rates. The mechanism of “process zone heating” might be generalised successfully to explain the genesis of magmas on regions as wide

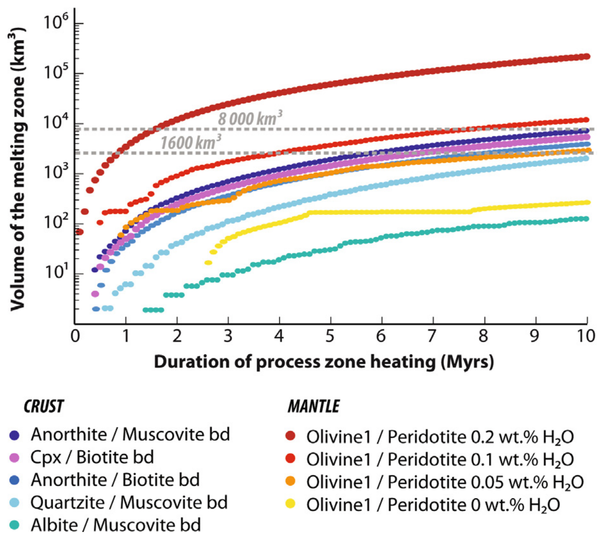

Fig. 8. Evolution of the volumes of crustal and mantle rocks whose temperature exceed their melting point for various pairs of rheology/solidus. Blue, green and magenta colours correspond to crustal combinations, red, orange and yellow ones to mantle ones. A volume of magma equivalent to the one of Bingöl/Turna volcanism (800 km^3) can be produced by reaching melting temperatures on a volume of rocks of, 1600 km^3 if the melt fraction is 50%, or 8000 km^3 if the melt fraction is 10%. See discussion in the text. (For interpretation of the references to colour in this figure legend, the reader is referred to the web version of this article.)

as the Anatolian and Tibetan plateaus. The challenge is to develop a deformation model that takes into account the heterogeneity of the deformation at different scales, not focusing only on major faults complexities.

6. Conclusion

Although this contribution opens new questions, and clearly further work is required to refine the general framework proposed here, it suggests that process zone heating is a viable mechanism of magma genesis in the lithosphere and should be investigated further. More efficient than strain heating along planar faults or shear zones, and than viscous heating over widely deforming areas, process zone heating emerges as a partial melting mechanism that is specific to the lithosphere. We have demonstrated the potential of this concept at an important strike-slip, strike-slip junction in a continental collision zone. According to our calculations, strain heating within the process zone that develop due to kinematic incompatibility can modify the thermal equilibrium of the lithosphere enough to produce thermal metamorphism, lead to partial melting of the crust and mantle and produce a voluminous bimodal magmatism. The approach should now be transposed to other geodynamic contexts.

Acknowledgements

MD thanks IPGP and ERC DISPERSE project (Grant No. 269586) for financial support and P. Tapponnier, C. Jaupart, R. Ryerson and C. Sammis for useful comments at various stages of this work. This is IPGP contribution number 3506.

Appendix A. Supplementary material

Supplementary material related to this article can be found online at http://dx.doi.org/10.1016/j.epsl.2014.03.002.

References

Amelung, F., King, G.C.P., 1997a. Large scale tectonic deformation inferred from small earthquakes. Nature 386, 702.
Amelung, F., King, G.C.P., 1997b. Earthquake scaling laws for creeping and non-creeping faults. Earth Planet. Sci. Lett. 24 (5), 507.
Angus, D.A., Wilson, D.C., Sandvol, E., Ni, J.F., 2006. Lithospheric structure of the Arabian and Eurasian collision zone in eastern Turkey from S-wave receiver functions. Geophys. J. Int. 166 (3), 1335.
Armijo, R., Flerit, F., King, G., Meyer, B., 2004. Linear elastic fracture mechanics explains the past and present evolution of the Aegean. Earth Planet. Sci. Lett. 217 (1–2), 1–85.
Armijo, R., Meyer, B., Hubert, A., Barka, A., 1999. Westward propagation of the North Anatolian fault into the northern Aegean: Timing and kinematics. Geology 27 (3), 267.
Ashby, M.F., Verrall, R.A., 1978. Micromechanisms of flow and fracture, and their relevance to the rheology of the Upper Mantle. Philos. Trans. R. Soc. Lond. Ser. A, Math. Phys. Sci. 288 (1350), 59.
Bowman, D., King, G., Tapponnier, P., 2003. Slip partitioning by elastoplastic propagation of oblique slip at depth. Science 300 (5622), 1121.
Brune, J.N., Henyey, T.L., Roy, R.F., 1969. Heat flow, stress, and rate of slip along the San Andreas Fault, California. J. Geophys. Res. 74, 3821.
Buket, E., Temel, A., 1998. Major-element, trace-element, and Sr–Nd isotopic geochemistry and genesis of Varto Mus volcanic rocks, Eastern Turkey. J. Volcanol. Geotherm. Res. 85 (1–4), 1–405.
Bürgmann, R., Dresen, G., 2008. Rheology of the lower crust and upper mantle: Evidence from rock mechanics, geodesy, and field observations. Annu. Rev. Earth Planet. Sci. 36, 531.
Byerlee, J.D., 1978. Friction of rocks. Pure Appl. Geophys. 116, 615.
Bystricki, M., Mackwell, S., 2001. Creep of dry clinopyroxene aggregates. J. Geophys. Res. 106 (B7), 13,443.
Chester, J.S., Chester, F.M., Kronenberg, A.K., 2005. Fracture surface energy of the Punchbowl fault, San Andreas system. Nature 437 (7055), 133.
Conrad, C.P., 2000. Convective instability of thickening mantle lithosphere. Geophys. J. Int. 143 (1), 52–70.
Cowgill, E., Yin, A., Arrowsmith, J.R., Feng, W.X., Shuanhong, Z., 2004. The Akato Tagh bend along the Altyn Tagh fault, northwest Tibet 1: Smoothing by vertical-axis rotation and the effect of topographic stresses on bend-flanking faults. Geol. Soc. Am. Bull. 116 (11–12), 1423.
Cowie, P.A., Scholz, C., 1992. Growth of faults by accumulation of seismic slip. J. Geophys. Res. 97 (B11), 11.
Devès, M., 2010. Continental magmatism by shear heating in process zones at geometric complexities of fault systems. PhD thesis. Institut de Physique du Globe de Paris, France.
Devès, M., King, G.C.P., Klinger, Y., Amotz, A., 2011. Localised and distributed deformation in the lithosphere: Modelling the Dead Sea region in 3 dimensions. Earth Planet. Sci. Lett. 308, 172.
England, P., McKenzie, D., 1982. A thin viscous sheet model for continental deformation. Geophys. J. R. Astron. Soc. 70 (2), 295–321.
Field, E.H., et al., 2013. Uniform California earthquake rupture forecast, Version 3 (UCERF3). USGS Open-File Report 2013-1165.
Flerit, F., Rolando, A., King, G., Meyer, B., 2004. The mechanical interaction between the propagating North Anatolian Fault and the back-arc extension in the Aegean. Earth Planet. Sci. Lett. 224 (3), 347.
Hartz, E.H., Podladchikov, Y.Y., 2008. Toasting the jelly sandwich: The effect of shear heating on lithospheric geotherms and strength. Geology 36 (4), 331.
Houseman, G., England, P., 1986. Finite strain calculations of continental deformation; method and general results for convergent zones. J. Geophys. Res. 91, 3651–3663.
Hubert-Ferrari, A., Armijo, R., King, G., Meyer, B., Barka, A., 2002. Morphology, displacement, and slip rates along the North Anatolian Fault, Turkey. J. Geophys. Res. 107 (B10), 2235.
Hubert-Ferrari, A., King, G., Manighetti, I., Armijo, R., Meyer, B., Tapponnier, P., 2003. Long-term elasticity in the continental lithosphere; modelling the Aden Ridge propagation and the Anatolian extrusion process. Geophys. J. Int. 153 (1), 111.
Hubert-Ferrari, A., King, G., Van der Woerd, J., Villa, I., Altunel, E., Armijo, R., 2009. Long-term evolution of the North Anatolian Fault: new constraints from its eastern termination. Geol. Soc. (Lond.) Spec. Publ. 311 (1), 133.
Ilkiçsik, O.M., 1995. Regional heat flow in western Anatolia using silica temperature estimates from thermal springs. Tectonophysics 244 (1–3), 175.
Jaupart, C., Mareschal, J.C., 2007. Crust and lithosphere dynamics. In: Treatrise on Geophysics, vol. 6. Elsevier, p. 217. Chapter 5.
Jolivet, M., Brunel, M., Seward, D., Xu, Z., Yang, J., Malavieille, J., Roger, F., Leyreloup, A., Arnaud, N., Wu, C., 2003. Neogene extension and volcanism in the Kunlun Fault Zone, northern Tibet: New constraints on the age of the Kunlun Fault. Tectonics 22 (5), 1052.
Karato, S., 2008. Deformation of Earth Materials – An Introduction to the Rheology of Solid Earth. Cambridge University Press.
Karato, S.I., Wu, P., 1993. Rheology of the upper mantle – A synthesis. Science 260 (5109), 771.
Katz, R.F., Spiegelman, M., Langmuir, C.H., 2003. A new parameterization of hydrous mantle melting. Geochem. Geophys. Geosyst. 4 (9), 1073.

Kincaid, C., Silver, P., 1996. The role of viscous dissipation in the orogenic process. Earth Planet. Sci. Lett. 142 (3–4), 271.
King, G., Nabelek, J., 1985. Role of fault bends in the initiation and termination of earthquake rupture. Science 228, 984.
King, G.C.P., Brewer, J., 1983. Fault related folding near the Wind River thrust, Wyoming, USA. Nature 306, 147.
King, G.C.P., Devès, M., 2015. Fault interaction, earthquake stress changes, and the evolution of seismicity. In: Schubert, G. (Ed.), Treatrise on Geophysics. 2nd edition. Elsevier, Oxford. Chapter 77.
Kohlstedt, D.L., Evans, B., Mackwell, S.J., 1995. Strength of the lithosphere: Constraints imposed by laboratory experiments. J. Geophys. Res. 100 (17), 587.
Korenaga, J., Karato, S.I., 2008. A new analysis of experimental data on olivine rheology. J. Geophys. Res. 113, B02403.
Lachenbruch, A.H., Sass, J.H., 1980. Heat flow and energetics of the San Andreas fault zone. J. Geophys. Res. 85 (B11), 6185.
Leloup, P.H., Ricard, Y., Battaglia, J., Lacassin, R., 1999. Shear heating in continental strike-slip shear zones: Model and field examples. Geophys. J. Int. 136 (1), 19.
Lockner, D.A., Okubo, P.G., 1983. Measurements of frictional heating in granite. J. Geophys. Res. 88 (B5), 4313.
Lopez, S., Castro, A., 2001. Determination of the fluid-absent solidus and supersolidus phase relationships of MORB-derived amphibolites in the range 4–14 kbars. Am. Mineral. 86 (11–12), 1396.
McCaffrey, R., Zwick, P.C., Bock, Y., Prawirodirdjo, L., Genrich, J.F., Stevens, C.W., Subarya, C., 2000. Strain partitioning during oblique plate convergence in northern Sumatra: Geodetic and seismologic constraints and numerical modeling. J. Geophys. Res. 105 (B12), 28363.
McClusky, S., Balassanian, S., Barka, A., Demir, C., Ergintav, S., Georgiev, I., Gurkan, O., Hamburger, M., Hurst, K., Kahle, H., et al., 2000. Global Positioning System constraints on plate kinematics and dynamics in the eastern Mediterranean and Caucasus. J. Geophys. Res. 105 (B3), 5695.
McClusky, S., Reilinger, R., Mahmoud, S., Ben Sari, D., Tealeb, A., 2003. GPS constraints on Africa (Nubia) and Arabia plate motions. Geophys. J. Int. 155 (1), 126.
McKenzie, D.P., Morgan, W.J., 1969. Evolution of triple junctions. Nature 224, 125.
Miller, C., Schuster, R., Klötzli, U., Frank, W., Purtscheller, F., 1999. Post-collisional potassic and ultrapotassic magmatism in SW Tibet: geochemical and Sr–Nd–Pb–O isotopic constraints for mantle source characteristics and petrogenesis. J. Petrol. 40 (9), 1399–1424.
Morency, C., Doin, M.P., 2004. Numerical simulations of the mantle lithosphere delamination. J. Geophys. Res.: Solid Earth (1978–2012) 109 (B3).
Nabelek, P.I., Liu, M., 2004. Petrologic and thermal constraints on the origin of leucogranites in collisional orogens. Trans. R. Soc. Edinb. Earth Sci. 95 (1–2), 73.
Nabelek, P.I., Whittington, A.G., Hofmeister, A.M., 2010. Strain heating as a mechanism for partial melting and ultrahigh temperature metamorphism in convergent orogens: Implications of temperature-dependent thermal diffusivity and rheology. J. Geophys. Res. 115, B12417.
Okada, Y., 1992. Internal deformation due to shear and tensile faults in a half-space. Bull. Seismol. Soc. Am. 82 (2), 1018.
Paterson, M.S., Wong, T., 2005. Experimental Rock Deformation – The Brittle Field. Springer Verlag.
Pearce, J.A., Bender, J.F., De Long, S.E., Kidd, W.S.F., Low, P.J., Güner, Y., Saroglu, F., Yilmaz, Y., Moorbath, S., Mitchell, J.G., 1990. Genesis of collision volcanism in Eastern Anatolia, Turkey. J. Volcanol. Geotherm. Res. 44 (1–2), 189.
Peltzer, G., Tapponnier, P., 1988. Formation and evolution of strike-slip faults, rifts, and basins during the India–Asia collision – An experimental approach. J. Geophys. Res. 93 (B12), 15085.
Ranalli, G., Murphy, D., 1987. Geological stratification of the lithosphere. Tectonophysics 132, 281.
Reilinger, R., McClusky, S., Vernant, P., Lawrence, S., Ergintav, S., Cakmak, R., Ozener, H., Kadirov, F., Guliev, I., Stepanyan, R., et al., 2006. GPS constraints on continental deformation in the Africa–Arabia–Eurasia continental collision zone and implications for the dynamics of plate interactions. J. Geophys. Res. 111 (B5), B05411.
Ricard, Y., Froidevaux, C., Hermance, J.F., 1983. Model heat flow and magnetotellurics for the San Andreas and oceanic transform faults. Ann. Geophys. 1, 47.
Rolandone, F., Jaupart, C., 2002. The distributions of slip rate and ductile deformation in a strike–slip shear zone. Geophys. J. Int. 148 (2), 179.
Rosenberg, C.L., 2004. Shear zones and magma ascent: a model based on a review of the Tertiary magmatism in the Alps. Tectonics 23 (3).
Rybacki, E., Gottshalk, M., Wirth, R., Dresen, G., 2006. Influence of water fugacity and activation, on the flow properties of fine-grained anorthite aggregates. J. Geophys. Res. 111, B03203.
Scholz, C.H., 2002. The Mechanics of Earthquakes and Faulting (Book). Cambridge Univ. Press.
So, B.-D., Yuen, D.A., 2013. Influences of temperature-dependent thermal conductivity on surface heat flow near major faults. Geophys. Res. Lett. 40 (15), 3868–3872. http://dx.doi.org/10.1002/grl.50780.
Stocker, R.L., Ashby, M.F., 1973. On the rheology of the upper mantle. Rev. Geophys. 11 (2), 391.
Tapponnier, P., Zhiqin, X., Roger, F., Meyer, B., Arnaud, N., Wittlinger, G., Jingsui, Y., 2001. Oblique stepwise rise and growth of the Tibet Plateau. Science 294 (5547), 1671.
Thompson, A.B., Connolly, J.A.D., 1995. Melting of the continental crust: some thermal and petrological constraints on anatexis in continental collision zones and other tectonic settings. J. Geophys. Res. 100 (15), 565.
Turner, S., Arnaud, N., Liu, J., et al., 1996. Post-collision, shoshonitic volcanism on the Tibetan Plateau: implications for convective thinning of the lithosphere and the source of ocean island basalts. J. Petrol. 37 (1), 45–71.
Van Hunen, J., Allen, M.B., 2011. Continental collision and slab break-off: A comparison of 3-D numerical models with observations. Earth Planet. Sci. Lett. 302 (1), 27–37.
Weinberg, R.F., Sial, A.N., Mariano, G., 2004. Close spatial relationship between plutons and shear zones. Geology 32 (5), 377.
Wittlinger, G., Tapponnier, P., Poupinet, G., Mei, J., Danian, S., Herquel, G., Masson, F., 1998. Tomographic evidence for localized lithospheric shear along the Altyn Tagh fault. Science 282 (5386), 74–76.
Whittington, A.G., Hofmeister, A.M., Nabelek, P.I., 2009. Temperature-dependent thermal diffusivity of the Earth's crust and implications for magmatism. Nature 458 (7236), 319.
Yuen, D.A., Fleitout, L., Schubert, G., Froidevaux, C., 1978. Shear deformation zones along major transform faults and subducting slabs. Geophys. J. R. Astron. Soc. 54 (1), 93–119.
Zhang, L.S., Schärer, U., 1999. Age and origin of magmatism along the Cenozoic Red River shear belt, China. Contrib. Mineral. Pet. J. 134 (1), 67.
Zor, E., Sandvol, E., Gurbuz, C., Turkelli, N., Seber, D., Barazangi, M., 2003. The crustal structure of the East Anatolian plateau (Turkey) from receiver functions. Geophys. Res. Lett. 30 (24), 8044.